Desalination and Water Treatment
www.deswater.com

doi: 10.5004/dwt.2023.29824

310 (2023) 200–211
October

Adsorption properties of carboxymethyl cellulose/carbon hydrogel for copper and methylene blue

Keke Chen[a,b]

[a]*Henan Photoelectrocatalytic Material and Micro-nano Application Technology Academician Workstation, Xinxiang University, Xinxiang, Henan 453003, PR China, email: Chenkk820928@xxu.edu.cn*
[b]*College of Chemistry and Materials Engineering, Xinxiang University, Xinxiang, Henan 453003, PR China*

Received 11 February 2023; Accepted 16 July 2023

ABSTRACT

Carboxymethyl cellulose/biochar/polyacrylic acid composite (PAA/CMC/GBC) was prepared by hydrothermal synthesis of carboxymethyl cellulose and acrylic acid with ginger as raw material. The PAA/CMC/GBC were characterized by scanning electron microscopy, Fourier-transform infrared spectroscopy and X-ray photoelectron spectroscopy (XPS). The adsorption capacity of PAA/CMC/GBC for Cu^{2+} and methylene blue was significant (maximum adsorption capacity at 25°C was 170 mg·g^{-1} for Cu^{2+} and 110 mg·g^{-1} for methylene blue), and showed good adsorption performance in a wide range of pH values (pH 2–12). The pseudo-second-order kinetics and Langmuir isotherm model are more consistent with the actual adsorption process. The results of XPS show that electrostatic attraction is the main adsorption mechanism of PAA/CMC/GBC for methylene blue (MB) adsorption, and metal complexation is the main adsorption mechanism of PAA/CMC/GBC for Cu adsorption. In addition, PAA/CMC/GBC adsorbents also showed good cyclic stability after repeated use. Therefore, PAA/CMC/GBC can be used as an efficient and environmentally friendly adsorbent to remove Cu^{2+} and MB dyes from aqueous solutions.

Keywords: Adsorption; Water treatment; Biochar; Carboxymethyl cellulose

1. Introduction

Azo dyes (a class of organic compounds connected to aryl groups at both ends of azo groups) are the most widely used synthetic dyes in textile and clothing dyeing processes, used for dyeing and printing of a variety of natural and synthetic fibers, and also used in the coloring of paints, plastics, rubber, etc. [1]. Under special conditions, it can decompose and produce more than 20 kinds of carcinogenic aromatic amines, which change the DNA structure of the human body through activation, cause lesions and induce cancer. The main source of heavy metal pollution is industrial pollution, followed by traffic pollution and domestic garbage pollution. Industrial pollution is mostly discharged into the environment through waste residues, wastewater and waste gas, which are enriched in people and animals and plants, thus causing great harm to the environment and human health [2]. The treatment of industrial pollution can reduce its pollution through some technical methods and management measures, and finally reach the emission standards of pollutants [3–5]. There are a variety of biological, chemical and physical methods available to remove azo dyes from wastewater, including biodegradation, chemical reduction and adsorption [1].

Methylene blue (MB) is one of the most commonly used cationic dyes, which can be used for dyeing cotton, linen, silk, paper and bamboo. Although MB is not highly toxic, it can damage organs such as the kidneys, brain, and liver, and cause water pollution. At the same time, the chemical

structure of MB is complex and non-biodegradable, which will block the passage of sunlight, thus negatively affecting the aquatic environment. Copper(II) pollution mainly comes from copper mines, copper pipes, electroplating, and wastewater treatment plants. Copper is toxic and carcinogenic, with adverse effects on the liver, brain, and central nervous system [5]. The above two types of pollution are the most common water pollutants, and in reality, improper treatment of pollution is likely to lead to mixed pollution, which leads to more serious water pollution. Although biodegradation method and chemical reduction method have been widely used, these methods still have disadvantages such as low efficiency, high cost and not environmental protection. Adsorption is considered to be one of the most promising methods for the treatment of heavy metals and dyes. Asgari and Sahebi [6] prepared activated carbon CAC using *Phoenix* flower fruit pit as raw material, which was used to remove methylene blue (MB) dye from water, and the maximum adsorption capacity for MB reached 478.32 mg·g^{-1}. Foroutan et al. [7] successfully synthesized walnut shell ash (WSA)/starch/Fe_3O_4 magnetic nanocomposites by chemical deposition method for removing Cu(II) from groundwater. WSA and WSA/starch/Fe_3O_4 have the highest adsorption capacity of Cu(II). They were 29.0 and 45.4 mg·g^{-1}, respectively.

Nowadays, many scholars focus on the use of natural materials for preparation, which can reduce costs and be low-carbon and environmentally friendly. Carboxymethyl cellulose (CMC) is a natural material for preparing adsorbents. It is a hydrogel matrix with high water solubility, wide availability and low cost [8–10]. It contains a large number of active groups (–OH and –COOH). In addition, CMC can be cross-linked with polyvalent metal cations (such as Fe^{3+}, Al^{3+}, La^{3+}, etc.) to prepare a three-dimensional network structure and relatively stable and firm gel structure [11,12]. Gao et al. [13] prepared carboxymethyl GO (GOCOOH) complex adsorbent based on CMC microspheres for adsorption and removal of cationic MB dyes. The maximum adsorption capacity is 180.32 mg·g^{-1} [13]. Wang and Wei [14] prepared PAA/CMC/GBC hydrogels using polyethylene glycol as pore-forming agent by ionic crosslinking method to remove phosphate from aqueous solution. Yu et al. [15] studied and developed graphene oxide/CMC nanofiber composite fibers as an efficient and durable adsorbent for capturing heavy metal ions in wastewater. These studies show that CMC is a very practical adsorption material.

Ginger is a perennial herb with a high carbon content and a promising prospect for biochar preparation. It has been reported that biochar made from waste ginger root can remove pollutants from wastewater. The research on converting biological roots into treatment dyes has become one of the trends in the development of green materials [16–18]. Eltaweil et al. [19] reported the feasibility of simultaneously removing Cu(II), Pb(II) and Ni(II) ions from aqueous solution with three sorbents: ginger, alkaline ginger and acid ginger under different experimental parameters.

Traditional studies on adsorbents focus on one of heavy metal ions or organic dyes [20,21], and there are few studies involving the combination of the two pollutants and the adsorption relationship between the two pollutants. In this study, carboxymethyl cellulose/biochar/polyacrylic acid composite (PAA/CMC/GBC) was synthesized from ginger with carboxymethyl cellulose and acrylic acid under different experimental parameters for adsorption of Cu^{2+} and MB. The adsorption process of Cu^{2+} and MB by PAA/CMC/GBC was studied, and the adsorption relationship between the two existed at the same time was proposed.

2. Materials and methods

2.1. Materials and reagents

Ginger comes from the wet market in Xinxiang City. Potassium hydroxide (KOH, AR), nitric acid (HNO_3, AR, 65% concentration), anhydrous ethanol (C_2H_6O, AR, 99.5% concentration), carboxymethyl cellulose ($[C_6H_7O_2(OH)_2OCH_2COONa]_n$, MW 700,000 (DS = 0.9), 2,500 ~ 4,500 mpa·s), acrylic acid ($C_3H_4O_2$, GC, 99% concentration), potassium persulfate ($K_2S_2O_8$, AR, 99.6% concentration), copper nitrate ($Cu(NO_3)_2$, AR, 99.5%), methylene blue ($C_{16}H_{18}N_3ClS$, AR, 98%) were purchased from Shanghai Macklin Biochemical Co., Ltd., (Shanghai, China). The water used in the experiment was purified from Hangzhou Wahaha Group Co., Ltd., (Hangzhou, China).

2.2. Preparation of adsorbents

2.2.1. Pretreatment with ginger biochar (C)

Ginger was treated by KOH activation method. Dried raw ginger (10 g) was cut into filaments, ultrasonically treated in the KOH solution for 1 h, and then left to stand overnight. After filtering out excess KOH, the treated ginger was placed in an oven until it was dried. The dried ginger was placed in a tubular furnace and heated at 400°C for 0.5 h, after which the temperature was raised to 800°C for 1 h at a rate of 300°C·h^{-1}. Next, the samples were allowed to cool down to room temperature naturally, after which they were repeatedly washed with deionized water and dried. The ginger samples were put into a prepared HNO_3 solution (5 mol·L^{-1}) and stirred continuously using a magnetic stirrer for 0.5 h. Then, the samples were left to stand and oxidize for 24 h. Finally, the samples were washed to neutral pH and dried for subsequent experiments. The resulting samples were named C.

CMC (weight 5 g) and C (weight 5 g) were added to water (volume 10 mL), and were stirred continuously until combining. Acrylic acid (volume 10 mL) was added, and the resulting mixture was stirred well. Then, potassium persulfate (weight 0.5 g) was added, and stirred continuously until dissolution. The mixture was heated in a 65°C water bath for 3 h. After the reaction, the product was washed with anhydrous ethanol 3 times, and then dried at 60°C for 12 h. Finally, PAA/CMC/GBC was obtained.

2.3. Characterization

The functional groups of the adsorbent in the 4,000–400 cm^{-1} range were characterized using a Fourier-transform infrared spectroscopy (FTIR-1500, Zhong Shi Walker (Tianjin) Technology Development Co.). The surface microstates of the adsorbent were characterized using a scanning electron microscope (KYKY-EM8100, CSCI Beijing, China). A thermal analyzer (DTG-60A, Shimadzu, Japan) was used for characterizing the adsorbent's thermal stability. The

surface charge of the adsorbent was characterized using a potentiostat (Zetasizer Ultra, Malvern Panaco, Germany).

2.4. Adsorption experiments

Firstly, solid adsorbent (weight 0.01 g) was added into a beaker of water (volume 50 mL), for adsorption experiments. After the adsorption equilibrium was reached, the supernatant was analyzed for determining the residual concentration. Each experimental data is the average of the three experiments. The adsorption amount of the two pollutants by the adsorbent was determined using Eq. (1).

$$q_e = \frac{\left(C_0 - C_e\right)V}{m} \tag{1}$$

where C_0 and C_e (mg·L^{-1}) correspond to the concentrations of Cu^{2+} and MB in the initial and equilibrium states of adsorption, respectively. Parameter V (mL) represents the solution volume participating in the experiment, and m (g) is the amount of adsorbent used.

2.5. Independent adsorption experiment

The adsorption of Cu^{2+} and MB by PAA/CMC/GBC alone was characterized at 20°C. To explore the effect of the adsorbent dosage on the adsorption performance, the following parameter values were used: adsorbent dose (0.01–0.06 g), pH (6), time (4 h), and concentration (Cu^{2+} concentration was 50 mg·L^{-1}, while the concentration of MB was 25 mg·L^{-1}). In the experiments exploring the effect of pH on the adsorption performance, the following parameter values were used: adsorbent dose (0.01 g), pH (2–6 for Cu^{2+} and 2–12 for MB), time (4 h), and concentration (50 mg·L^{-1} for Cu^{2+} and 25 mg·L^{-1} for MB). In the adsorption kinetics studies, the following parameter values were used: adsorbent dosage (0.01 g), pH (6), time (0–4 h), and concentration (Cu^{2+} concentration was 50 mg·L^{-1}, while the concentration of MB was 25 mg·L^{-1}). The parameter values for the adsorption isotherms were as follows: adsorbent dose (0.01 g), pH (6), time (4 h), and concentration (Cu^{2+} concentration was 5–30 mg·L^{-1}, while the concentration of MB was 50–100 mg·L^{-1}).

2.6. Competitive adsorption experiment

Mixed-adsorption experiments were carried out in this setting, considering the competitive adsorption behavior of Cu^{2+} and MB in the binary system. Cu^{2+} at initial concentrations of 0–25 mg·L^{-1} was adsorbed in the MB-Cu^{2+} binary system in the presence of MB (15 and 25 mg·L^{-1}). Similarly, the adsorption of MB (5–25 mg·L^{-1}) was measured for the Cu^{2+}-MB binary system in the presence of Cu^{2+} (15 and 25 mg·L^{-1}).

2.7. PAA/CMC/GBC regeneration experiment

After the adsorption equilibrium experiment, the saturated adsorbent loaded with Cu^{2+} and MB was collected. Subsequently, the desorption experiment was carried out in a 0.1 mol·L^{-1} HCl solution. After 24 h of desorption, the adsorbent was washed repeatedly and dried for the next adsorption cycle. The experimental conditions were set as follows: pH (6), dosage of adsorbent (0.01 g), time (4 h), concentration of adsorbent (Cu^{2+} concentration of 50 mg·L^{-1}, MB concentration of 25 mg·L^{-1}). In this experiment, PAA/CMC/GBC carried out a total of 5 adsorption–desorption cycle experiments. The cyclic adsorption efficiency was determined using Eq. (2),

$$\alpha_n = \frac{q_n}{q_0} \times 100\% \tag{2}$$

where q_0 is the first adsorption capacity of PAA/CMC/GBC adsorbent, and q_n is the n–1 adsorption capacity. α_n represents the (n–1)th cycle adsorption efficiency.

3. Results and discussion

3.1. Morphology and chemical characterization

Scanning electron microscopy (SEM) was used for observing the surface morphology of PAA/CMC/GBC, and the results are shown in Fig. 1A and B. The surface of the adsorbent presents well-developed pores, conducive to the adhesion of pollutants. In addition, it is evident that the surface of the adsorbent is uneven, which provides a more convenient internal condition for the adsorption of pollutants [22]. After successfully capturing MB, the surface morphology of PAA/CMC/GBC (Fig. 1C) changed significantly, from the initial pore structure to a striped stack. In contrast, the pores of PAA/CMC/GBC (Fig. 1D) were completely covered after the adsorption of Cu^{2+}, yielding the fold structure. These changes clearly demonstrate that both pollutants successfully adhered to the adsorbent [23].

Infrared spectroscopy is one of the most basic characterization methods. It determines changes in the positions and strengths of functional groups, before and after the adsorbents' synthesis. As shown in Fig. 2Ac, CMC exhibits an O–H stretching vibration peak at 3,416 cm^{-1}, N–H stretching vibration peak at 2,922 cm^{-1}, carboxyl asymmetric vibration peak at 1,601 cm^{-1}, carboxyl symmetric vibration peak at 1,415 cm^{-1}, C–H in-plane bending vibration peak at 1,324 and 1,048 cm^{-1}, bending vibration peak in the C–H plane at 1,324 cm^{-1}, and bending vibration peak outside the C–H plane at 1,048 cm^{-1} [24]. In Fig. 2Ab, C exhibits an O–H stretching vibration peak at 3,421 cm^{-1}, N–H stretching vibration peak at 2,968 cm^{-1}, C=O stretching vibration peak at 1,718 cm^{-1}, C–N stretching vibration peak at 1,523 cm^{-1}, C–H out-of-plane bending vibration peak at 1,041 cm^{-1}, and N–H out-of-plane bending vibration peak at 882 cm^{-1}. In Fig. 2b C–H vibration absorption peak appears at 2,954 cm^{-1}, C=O stretching vibration peak appears at 1,730 cm^{-1}, and C–O vibration absorption peak appears at 1,250 and 1,170 cm^{-1}. Fig. 2Aa shows that PAA/CMC/GBC exhibits the characteristic absorption peaks of CMC, C and PAA, with an O–H stretching vibration peak at 3,417 cm^{-1}, N–H stretching vibration peak at 2,940 cm^{-1}, C=O stretching vibration peak at 1,702 cm^{-1}, C–N stretching vibration peak at 1,572 cm^{-1}, carboxyl symmetry at 1,402 cm^{-1} vibration peak, C–H out-of-plane bending vibration peak at 1,050 cm^{-1}, and N–H out-of-plane bending vibration peak at 814 cm^{-1}. The FTIR results thus indicate that C and CMC can be grafted to the polyacrylic acid [25].

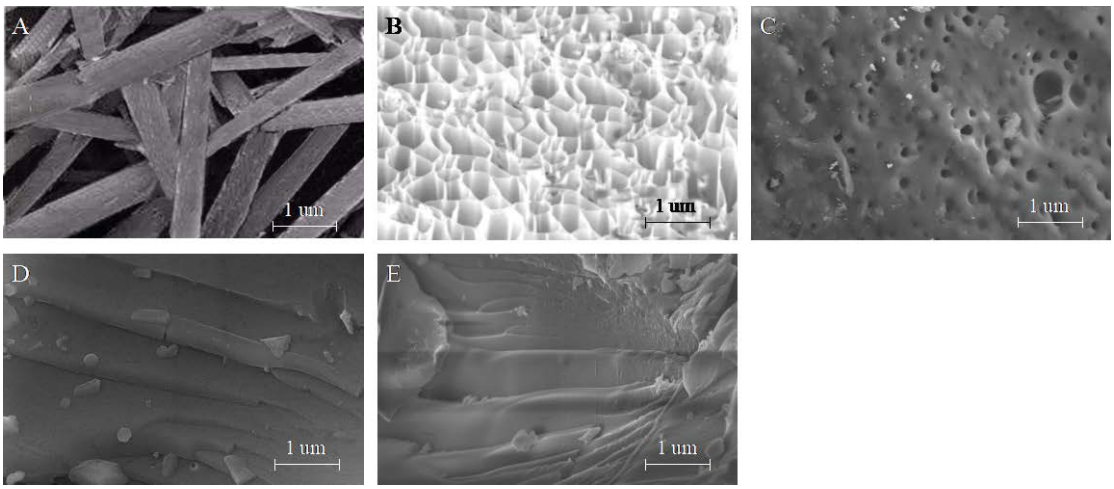

Fig. 1. Scanning electron microscopy of CMC (A), C (B), PAA/CMC/GBC (C), MB-PAA/CMC/GBC (D), and Cu^{2+}-PAA/CMC/GBC (E).

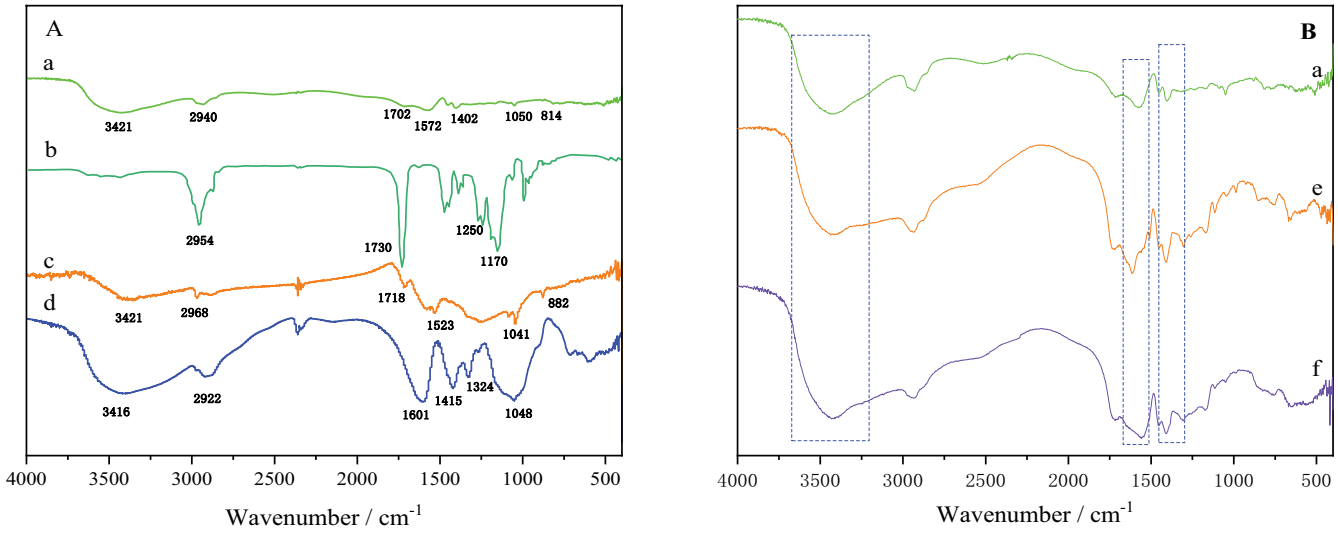

Fig. 2. Fourier-transform infrared (A) spectra of PAA/CMC/GBC (a), PAA (b), CMC (c), C (d) after adsorption Cu^{2+} (e), and MB (f).

In Figs. 2Ba, d, e, after the adsorption of Cu^{2+} and MB, the PAA/CMC/GBC FTIR absorption peaks exhibit changes in the O–H vibrational absorption peak, N–H vibrational absorption peak, and C=O vibrational absorption peak positions and peak intensities, indicating that these functional groups were involved in the adsorption process. The functionalities of the adsorbent did not change, indicating that the adsorbent maintained good stability after adsorption.

Considering the environmental thermal stability of the adsorbent in practical applications, the thermal stability of PAA/CMC/GBC was studied. As shown in Fig. 3B and C, the thermal decomposition behavior of CMC can be divided into two stages, according to the change of weight within the range of studied temperatures. Apart from the water loss below 250°C, above 250°C the change was mainly owing to the decomposition of the CMC backbone and owing to the removal of oxygen-containing functional groups. With respect to C, the weight loss for temperatures from room temperature up to 800°C was entirely owing to the evaporation of physically adsorbed or structured water. The thermogravimetry analysis results showed that the decomposition of PAA/CMC/GBC occurred in three stages: (1) the incipient reduced for temperatures in the 25°C–250°C range, which was attributed to the evaporation of adsorbed water; (2) the degradation in the 250°C–410°C range was owing to the breaking of the graft polymer chain and the polymer's pyrolysis, while the main weight loss in the 410°C–800°C range was owing to the decomposition of the main polymer chain; (3) at 800°C, all of the cross-linked chains broke and the polymer was completely decomposed.

3.2. Adsorption properties of the adsorbent

3.2.1. Effect of solution pH

pH significantly affects adsorption. pH can change the charge state on the adsorbent surface, and there is a competitive relationship with the adsorbate [26]. The Cu^{2+} solution

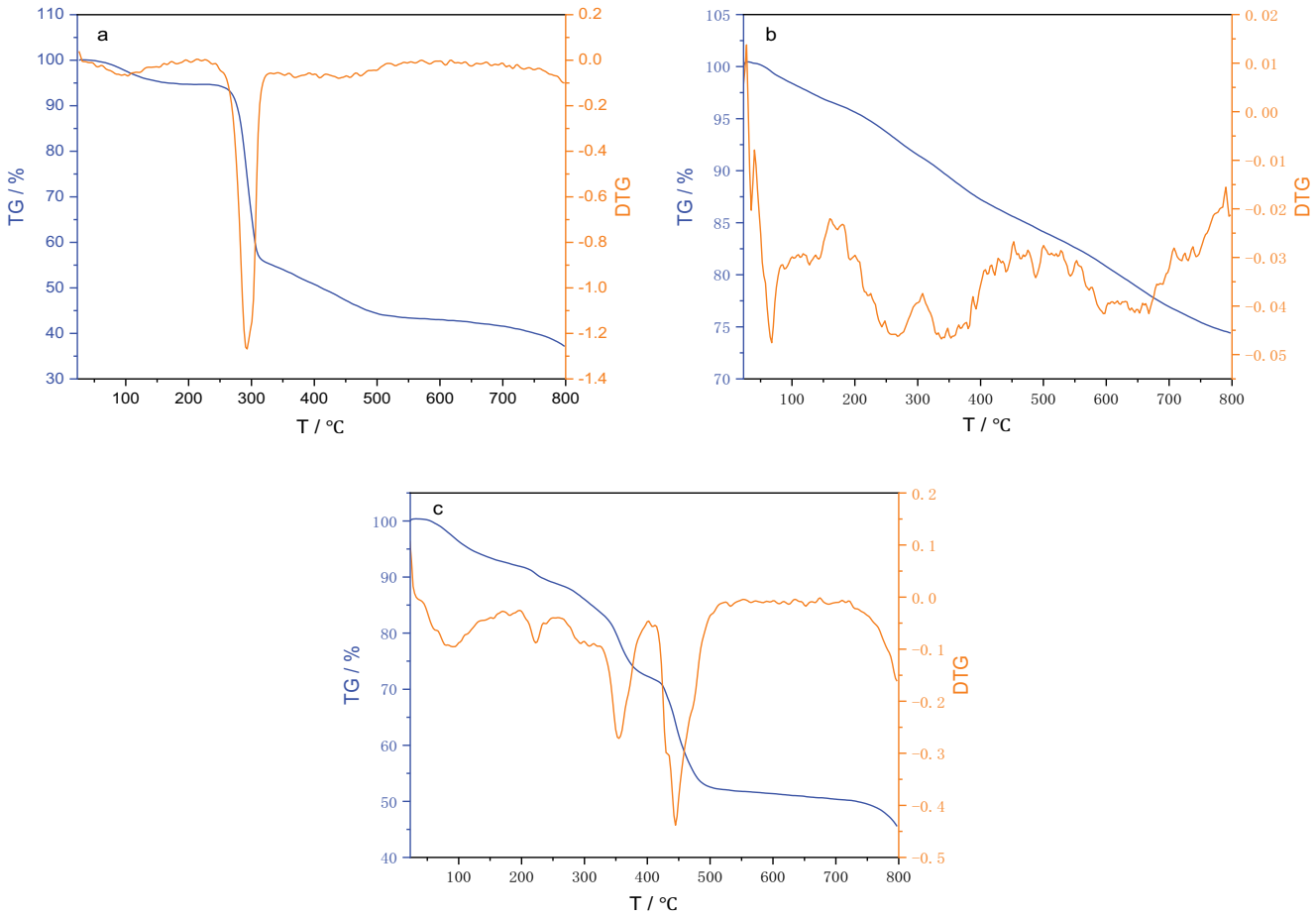

Fig. 3. Thermogravimetry and derivative thermogravimetry curves for CMC (a), C (b), and PAA/CMC/GBC (c).

appears to precipitate at pH = 6.89; therefore, pH > 6.89 is not suitable for studying the effect of pH on the adsorption performance. As shown in Fig. 4A, pH ≤ 3 was unfavorable for capturing Cu^{2+}, which was attributed to the preferential binding of the adsorbent to H^+ in solution. The adsorption capacity of the adsorbent for Cu^{2+} significantly improved with increasing pH, which was mainly attributed to the deprotonation of carboxyl groups and other reactive groups on the surface of the adsorbent when electrostatic attraction facilitated the adhesion of Cu^{2+} to the adsorbent [27]. For MB, the pH range of the study was set to 2–12. Fig. 4B shows that the adsorption capacity was low at pH < 3, whereas the adsorption capacity of PAA/CMC/GBC on MB remained at approximately 110 $mg \cdot g^{-1}$ for pH > 3. Combining these two results revealed that the optimal pH was 6. The effect of pH on the adsorption performance affected the surface charge state. As shown in Fig. 4C, the positive surface charge density of PAA/CMC/GBC decreased with increasing pH [28]. It is well known that for pH ≤ pH_{zpc} (zero-charge point), the adsorbent surface is positively charged and heavy-metal Cu exists as divalent cations, which explains the adsorption of Cu^{2+} and the basic dye MB at lower pH. Notably, pH had little effect on the adsorption of contaminants for pH > pH_{zpc}, suggesting that electrostatic attraction may not be the main mode of the Cu^{2+} and MB adsorption by the adsorbent [29]. Given the abundance of functional groups (carboxyl, hydroxyl, and amine groups) on the surface of the adsorbent, it is likely that the pollutants were coordinated with PAA/CMC/GBC through surface complexation for the pollutants' adsorption. In general, two cooperative mechanisms-electrostatic attraction and surface complexation-jointly promote adsorption.

3.2.2. Effect of the PAA/CMC/GBC dose

To further optimize the adsorption conditions, the effect of the adsorbent dose on the experimental results is shown in Fig. 4B. As the adsorbent dose increased from 0.01 to 0.06 g, the adsorption capacity dropped rapidly, indicating that the adsorption sites were not fully utilized for high adsorbent doses [30]. In general, an increase in the adsorbent dose inevitably leads to a large adsorption capacity; however, agglomeration occurs when a large dose of adsorbent is distributed in the solution, which leads to the underutilization of most sites. Thus, 0.01 g PAA/CMC/GBC was used in subsequent experiments, ensuring the maximal interaction between the adsorption sites and the pollutants [31].

3.2.3. Effect of the contact time and adsorption dynamics

To evaluate the removal rates of the two pollutants by the proposed adsorbent, the corresponding adsorption

capacities at different times were deliberately studied [32]. As shown in Fig. 5A and B, the adsorbent exhibited the same trend for the two pollutants; in both cases, rapid adsorption occurred in the initial stage, followed by slower adsorption toward the final equilibrium state. Evidently, the presence of a sufficient number of active sites ensured rapid initial adsorption, which later balanced out as the number of active sites gradually decreased [33]. Two kinetic models: a pseudo-first-order model and a pseudo-second-order model were established, for describing the rate-controlling step of the pollutants' adsorption process. These models were given by the following Eqs. (3) and (4):

Pseudo-first-order model:

$$q_t = q_e\left(1 - e^{-k_1 t}\right) \tag{3}$$

Pseudo-second-order model:

$$q_t = \frac{k_2 q_e^2 t}{1 + k_2 q_e t} \tag{4}$$

where q_e (mg·g^{-1}) and q_t (mg·g^{-1}) correspond to the adsorption amounts at equilibrium and at time t, respectively, while k_1 and k_2 represent the adsorption rate constants of the pseudo-first-order and pseudo-second-order models, respectively.

The parameters of the two models are listed in Table 1. The coefficient of determination (R^2) of the pseudo-second-order kinetic model for the removal of Cu^{2+} and MB from PAA/CMC/GBC was higher than that of the pseudo-first-order kinetic model [34,35]. In addition, the equilibrium adsorption capacity calculated according to the pseudo-second-level kinetic model deviated less from the experimental data, indicating that the adsorption process was better described by the pseudo-second-level kinetic model [36].

3.2.4. Effects of the pollutants' concentrations and adsorption isotherms

Adsorption isotherms capture the effect of the solution concentration on the adsorption capacity and the interaction between the adsorbed pollutants and the adsorbent [37]. Similar to the trend shown in Fig. 6A and B, the results for the adsorption isotherms showed that the adsorption capacity of Cu^{2+} and MB by PAA/CMC/GBC initially increased with the adsorbent concentration, and then reached equilibrium. When adsorption sites were sufficiently available, the driving force of the mass transfer increased with increasing

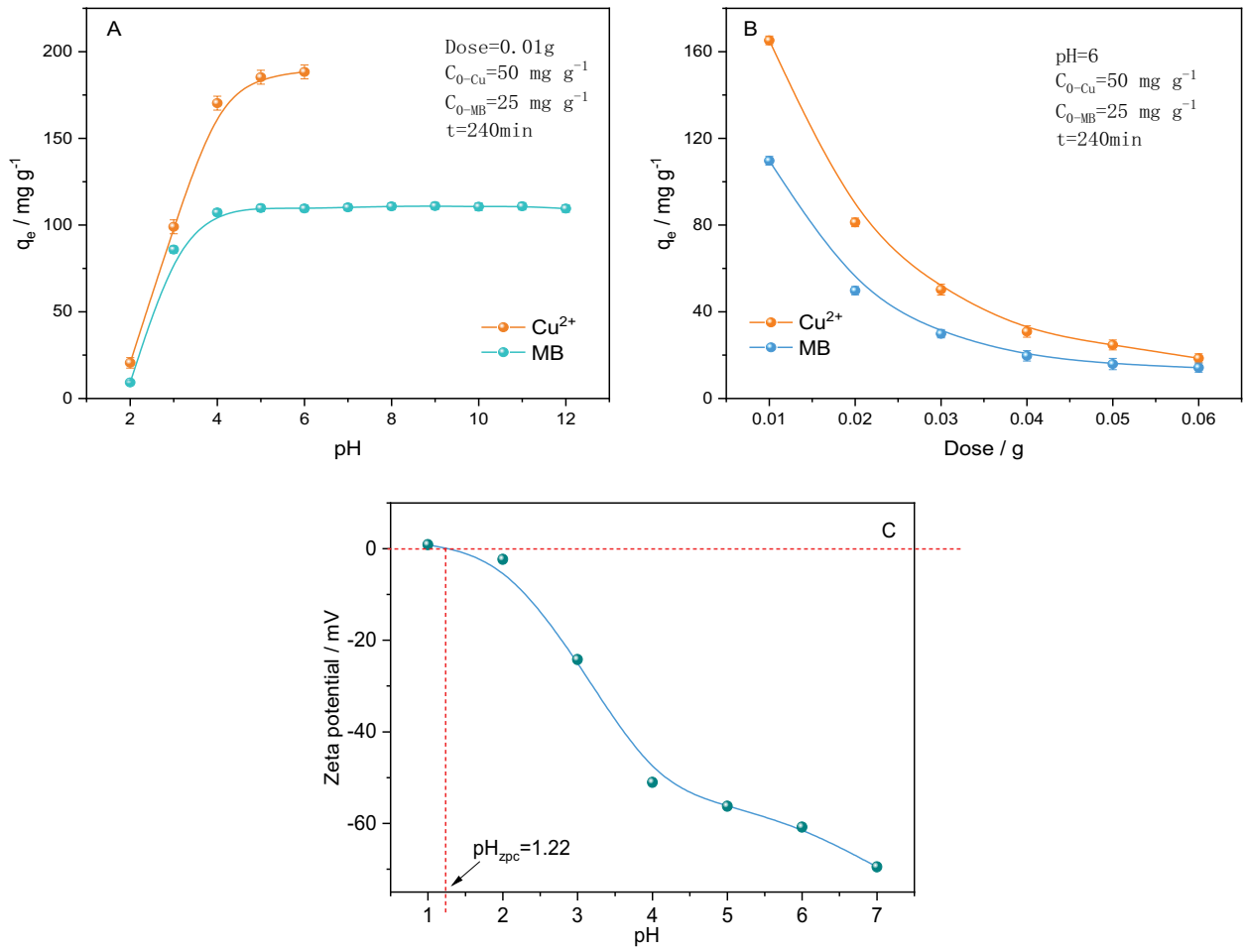

Fig. 4. Effect of pH on adsorption (A), effect of the PAA/CMC/GBC dose on adsorption (B), zeta potential of PAA/CMC/GBC at different pH (C).

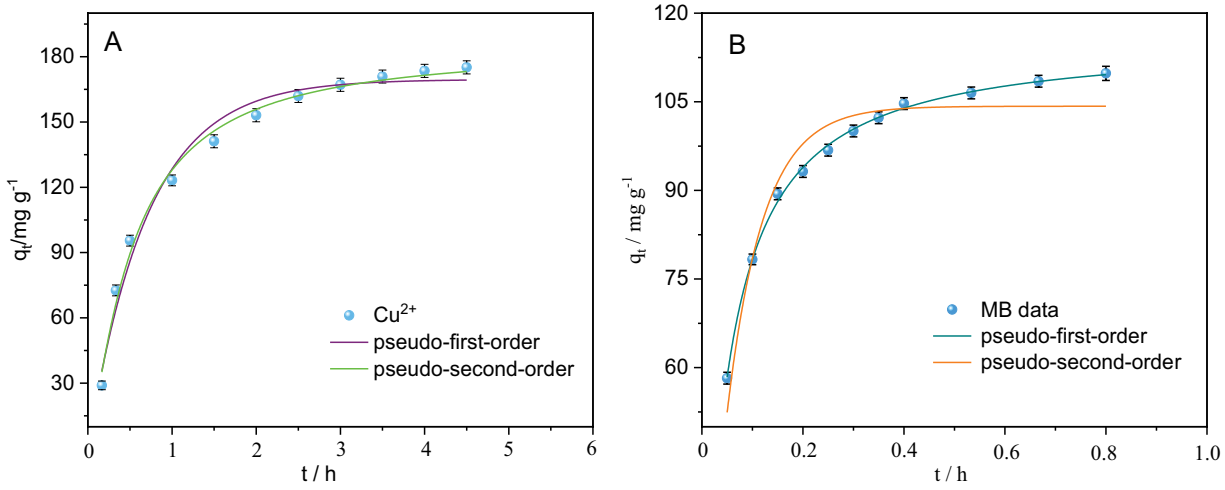

Fig. 5. Adsorption kinetics models of Cu^{2+} (A) and MB (B) by PAA/CMC/GBC.

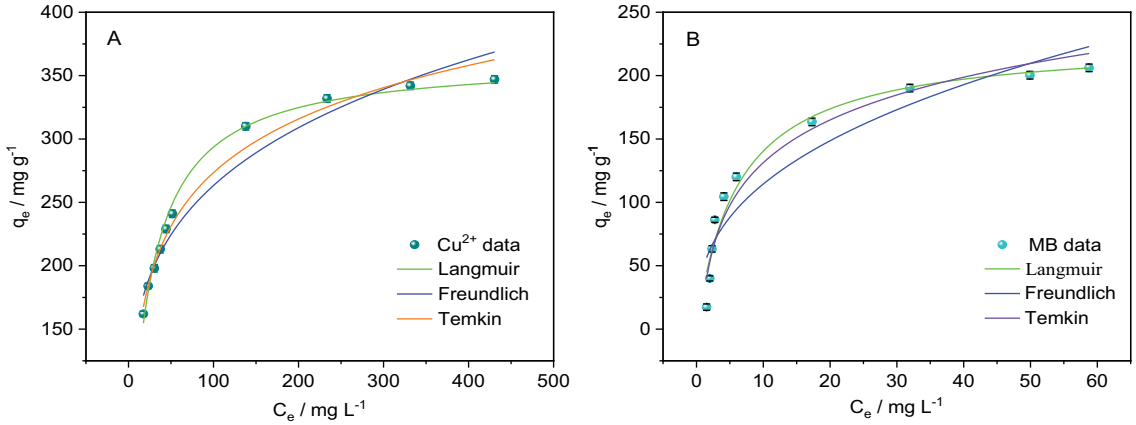

Fig. 6. Adsorption isotherms: Langmuir's, Freundlich's, and Temkin's.

Table 1
Kinetic constants of the adsorbents for Cu^{2+} and MB

Parameters	Cu^{2+}	MB
Pseudo-first-order		
q_e (mg·g^{-1})	169.5	104.2
k_1 (min^{-1})	0.024	0.233
R^2	0.983	0.938
Pseudo-second-order		
q_e (mg·g^{-1})	184.7	115.6
k_2 (g·mg^{-1}·min^{-1})	0.013	0.325
R^2	0.991	0.998

concentration, and at high concentrations the pollutants' molecules were more likely to bind to the adsorption sites. The isotherm data for the adsorption of Cu^{2+} and MB by PAA/CMC/GBC were simulated using two well-known isotherm models, captured by the following Eqs. (5)–(7):

Langmuir:

$$q_e = \frac{q_m K_L C_e}{1 + K_L C_e} \tag{5}$$

Freundlich:

$$q_e = K_F C_e^{1/n} \tag{6}$$

Temkin:

$$q_e = A + B \ln C_e \tag{7}$$

where C_e (mg·L^{-1}) is the concentration of adsorbed pollutants for equilibrium adsorption, q_e (mg·g^{-1}) is the adsorption capacity of PAA/CMC/GBC with respect to Cu^{2+} and MB in the adsorption equilibrium. K_L and K_F are the Langmuir and Freundlich constants related to the adsorption capacity, respectively. A (L·g^{-1}) and B are the constants of the Temkin model.

The fit results are shown in Fig. 6A and B, and the relevant kinetic parameters are listed in Table 2. The fit for the Langmuir model was closer to the experimental data;

in addition, the coefficient of determination (R^2) for the Langmuir model was higher than for the other models [38]. Thus, the Langmuir isotherm model adequately described the adsorption process in this study, indicating that the adsorption of Cu^{2+} and MB on PAA/CMC/GBC might have taken place on the monolayer.

3.3. Competitive adsorption

Mixed adsorption takes place in actual wastewater owing to its complex composition, and potential interactions between the different types of pollutants; therefore, it is necessary to conduct mixed-adsorption experiments [39]. For this purpose, adsorption experiments were carried out on Cu^{2+}-MB and MB-Cu^{2+} binary systems, for comparing the results with those obtained for mono-pollutant systems.

Fig. 7A shows the effect of different concentrations (0, 15, and 25 mg·g^{-1}) of Cu^{2+} on the adsorption of MB by PAA/CMC/GBC. At the same concentration of Cu^{2+}, the adsorption concentration of PAA/CMC/GBC on MB increased as the initial concentration of MB increased. As shown in Fig. 7A, the MB adsorption capacity of PAA/CMC/GBC increased with increasing concentration of (0, 15, and 25 mg·g^{-1}) Cu^{2+}. At the same concentration, the adsorption capacity of Cu^{2+} by PAA/CMC/GBC increased with an increase in the initial Cu^{2+} concentration. When the initial concentration of Cu^{2+} was 50 mg·g^{-1}, the adsorption capacity of Cu^{2+} by PAA/CMC/GBC increased from 170 to 195 mg·g^{-1} with increasing MB concentration, indicating that MB promoted the adsorption of Cu^{2+} by PAA/CMC/GBC. In summary, these binary-system experiments indicated that MB and Cu^{2+} mutually promoted adsorption.

Table 2
Isotherm parameters of the adsorbents for Cu^{2+} and MB

Type of pollutant	Cu^{2+}	MB
Langmuir		
q_m (mg·g^{-1})	363.3	227.9
K_L (L·mg^{-1})	0.042	0.190
R^2	0.992	0.948
Freundlich		
K_F (L·g^{-1})	91.09	48.12
$1/n$	0.231	0.376
R^2	0.958	0.872
Temkin		
A (mg·L^{-1})	–4.742	19.25
B	61.01	48.65
R^2	0.985	0.947

3.4. Adsorption mechanism

The adsorption of Cu^{2+} on PAA/CMC/GBC may be related to the complexation and electrostatic interactions between the oxygen-containing groups on PAA/CMC/GBC. As can be seen from the effect of pH on the adsorption capacity, the adsorption capacity of Cu^{2+} increases at pH values higher than pH_{pzc}. This indicates that negatively charged PAA/CMC/GBC can easily combine with positively charged Cu^{2+} through electrostatic attraction, thereby increasing the adsorption capacity. In addition, the increase in pH also led to the deprotonation of oxygen-containing groups on PAA/CMC/GBC, and the adsorbent allowed more functional groups to form complexes with Cu^{2+} [40,41].

High-resolution O_{1S} X-ray photoelectron (XPS) spectra of PAA/CMC/GBC (Fig. 8A) C=O and C–O/C=O groups revealed obvious deconvolution peaks at 532.5 and 532.0 eV, respectively. After the Cu^{2+} adsorption, the binding energies of C=O and C–O/C=O groups were 532.4 and 531.8 eV, respectively, and a Cu–O peak appeared at 530.8 eV, as shown in Fig. 8B. This indicates that the charge of these groups was transferred to Cu^{2+} after the adsorption, confirming that the C=O and C–O/C=O groups were the adsorption sites [42]. PAA/CMC/GBC could remove MB via two possible mechanisms. Hydrogen bonds exist between the –N= group on MB and the –OH and –COOH groups on the adsorbent. Second, there are π electrons in the aromatic ring of MB, which easily interact with the P electrons of PAA/CMC/GBC, thus increasing the adsorption capacity of MB.

The increase in the adsorption capacity of Cu^{2+} and MB in the binary system might be owing to the interaction

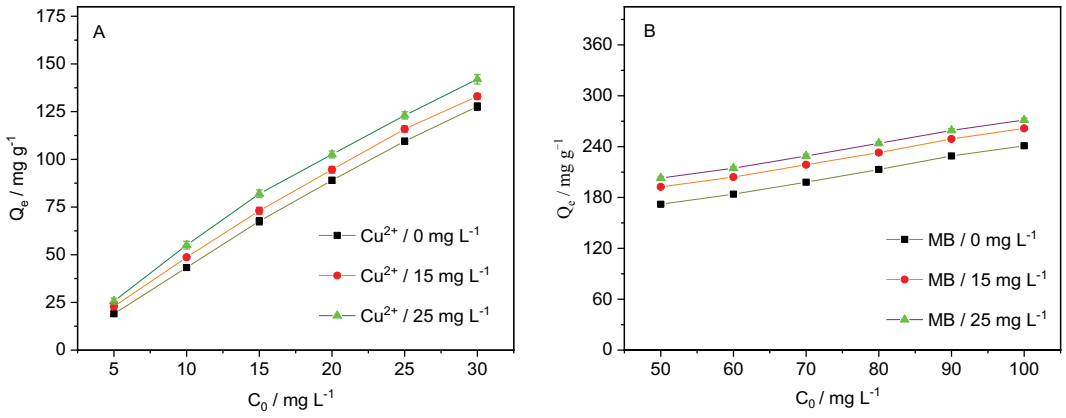

Fig. 7. Adsorption capacity of MB by PAA/CMC/GBC in the Cu^{2+}-MB system (A) and adsorption amount of Cu^{2+} by PAA/CMC/GBC in the MB-Cu^{2+} system (B).

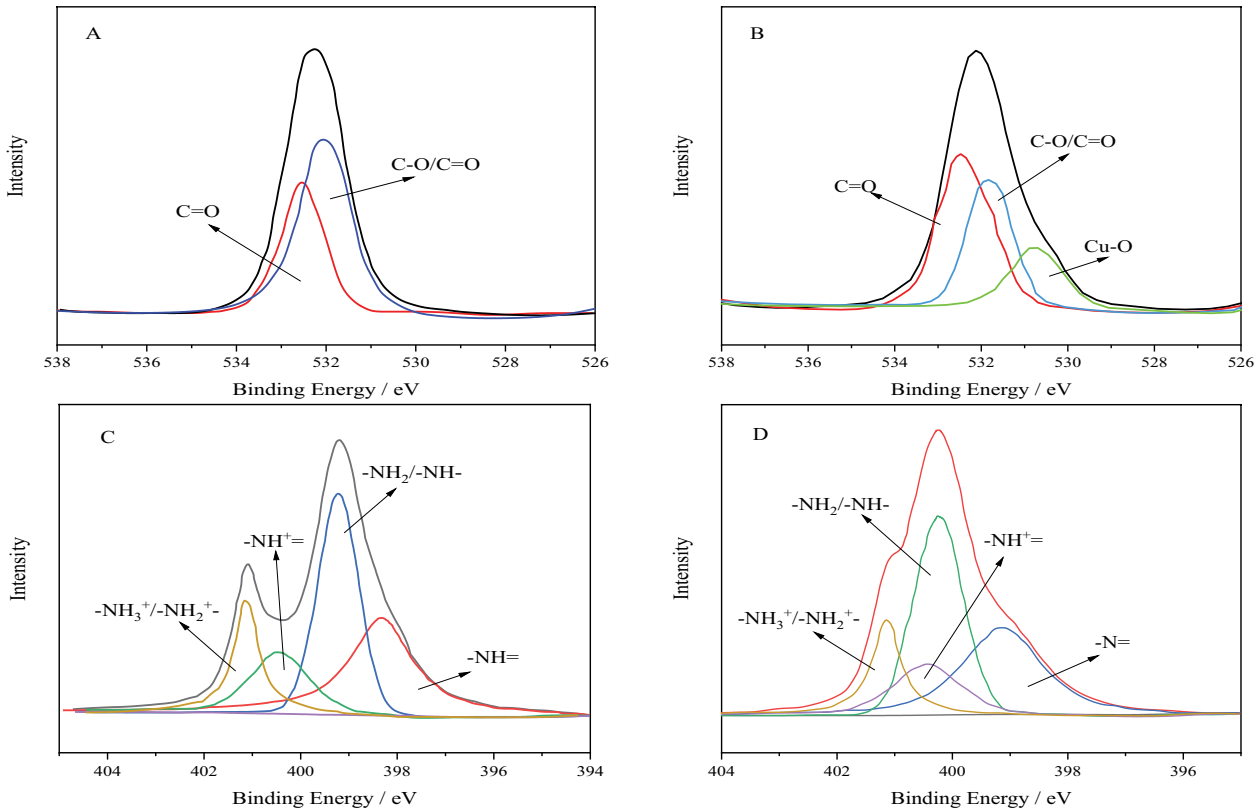

Fig. 8. X-ray photoelectron spectroscopy O1s (A, B), and N1s (C, D) spectra of PAA/CMC/GBC before and after Cu^{2+} (A, B), and MB (C, D) adsorption.

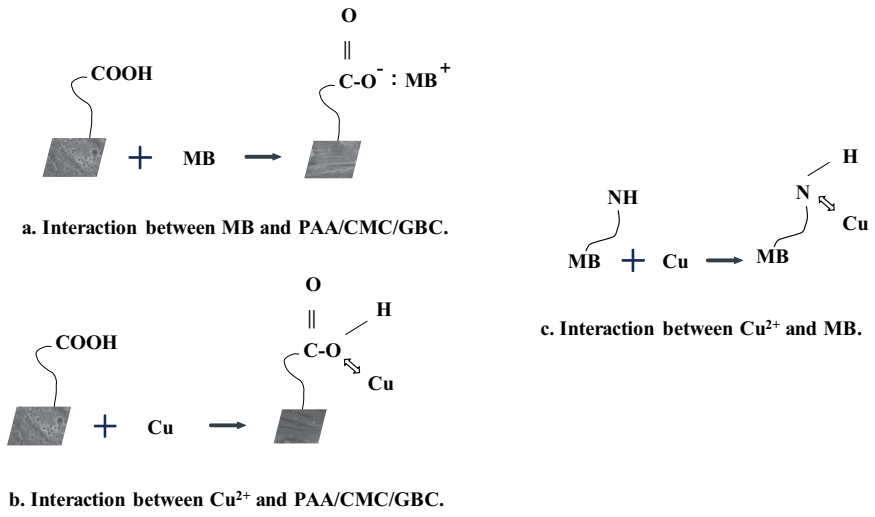

Fig. 9. Adsorption mechanism of Cu^{2+} and MB by PAA/CMC/GBC and interaction mechanism of Cu^{2+} and MB.

between the adsorbed Cu^{2+} (MB) and free MB (Cu^{2+}) in the solution. As shown in Fig. 8C, the N1s spectrum of the PAA/CMC/GBC-adsorbed MB reverted to four peaks at the binding energies of 398.3, 399.2, 400.4, and 401.1 eV corresponding to the –N=, $–NH_2$/–NH–, $–NH^+$=, and $–NH_3^+$/$–NH_2^+$– groups, respectively. When Cu^{2+} and MB were adsorbed on PAA/CMC/GBC at the same time, the peaks at 398.3 and 399.2 eV were 399.1 and 400.2 eV, respectively (Fig. 8D), indicating that the –N= and $–NH_2$/–NH– groups in MB were involved in the adsorption of Cu^{2+}. These results confirm that the adsorbed Cu^{2+} could chelate with the –N= and $–NH_2$/–NH– groups of free MB. Similarly, the –N= and $–NH_2$/–NH– groups adsorbing MB could also interact with free Cu^{2+} in the solution. Therefore, the Cu^{2+} and MB

Table 3
Comparison of adsorption capacities of several adsorbents for Cu^{2+} and MB

Adsorbent	Cu^{2+} ($mg \cdot g^{-1}$)	MB ($mg \cdot g^{-1}$)	Adsorption form	References
GBC/CMC-g-AA	170	110	Langmuir	This study
PAA/CTS/BC	111		Langmuir	[3]
HFO-001	89		/	[4]
UiO-66/GOCOOH@SA	343.49	490.72	Freundlich	[5]
CTS/CMC		65	/	[9]
HCB	99		Langmuir	[11]
F^{+}-MgO		10	/	[37]
cPAN-Ag		50	/	[41]
SPAN/PPy/ZnO_s		40	/	[41]

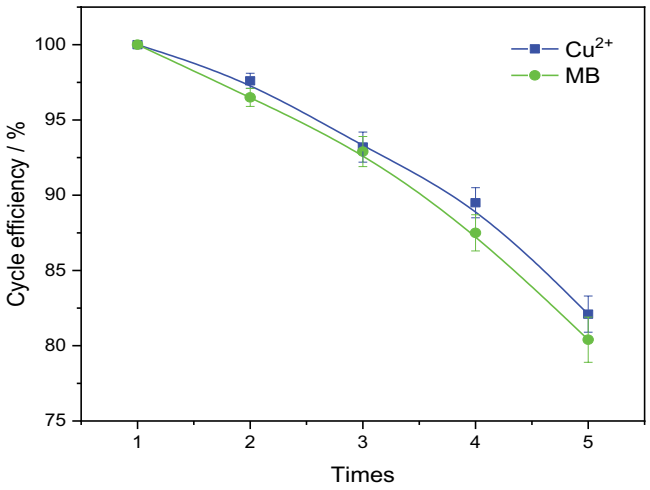

Fig. 10. Recycling performance of PAA/CMC/GBC during five cycles.

adsorption capacities increased in the binary system. The synergistic adsorption mechanisms of Cu^{2+} and MB based on the above analysis are shown in Fig. 9.

3.5. PAA/CMC/GBC regeneration experiment

An ideal adsorbent not only has excellent adsorption performance but also is stable and reusable. Considering actual applications, the adsorbent was subjected to multiple adsorption–desorption cycles, for determining its reusability. The results in Fig. 10 show that there was no obvious decrease in the adsorption capacity for Cu^{2+} and MB by PAA/CMC/GBC. Regardless of the adsorption of Cu^{2+} or MB, the adsorption efficiency remained above 80% after five cycles of experiments. The adsorbent did not completely desorb the contaminants in the multiple elution process, and there was still a small amount of residue, which is expected. Thus, PAA/CMC/GBC can be used as a highly efficient and reusable adsorbent for the purification of polluted water [43,44].

The Cu^{2+} and MB adsorption capacities of PAA/CMC/GBC were compared with those of other carbon adsorbents reported recently. Although the maximal adsorption performance of PAA/CMC/GBC for Cu^{2+} and MB was not the best among the listed results (Table 3), the comparison suggests that PAA/CMC/GBC can still be used as an efficient adsorbent.

4. Conclusion

In this study, PAA/CMC/GBC adsorbent was prepared by hydrothermal method. FTIR, SEM and TG analysis showed that the adsorbent was successfully synthesized. When pH = 6, adsorbent dose was 0.01 g and the time was 240 min, the maximum adsorption capacity of Cu^{2+} (initial concentration of 50 $mg \cdot L^{-1}$) was 170 $mg \cdot g^{-1}$, and that of MB (initial concentration of 25 $mg \cdot L^{-1}$) was 110 $mg \cdot g^{-1}$. The adsorption process followed the pseudo-second-order adsorption kinetics and Langmuir isothermal adsorption model. In the mixed solution of Cu^{2+} and MB, the two can promote the adsorption of each other. The good adsorption performance after 5 cycles indicates that PAA/CMC/GBC has excellent recyclable ability. In addition, ginger used in this study is an abundant and inexpensive raw material, indicating that PAA/CMC/GBC is cheap and has a greater application prospect.

Acknowledgements

This work was supported by the Scientific and Technological Research Projects of Henan Province (No. 222102320148).

References

[1] B. Ramavandi, S. Farjadfard, M. Ardjmand, Mitigation of orange II dye from simulated and actual wastewater using bimetallic chitosan particles: continuous flow fixed-bed reactor, J. Environ. Chem. Eng., 2 (2014) 1776–1784.
[2] G. Asgari, B. Ramavandi, S. Farjadfard, Abatement of azo dye from wastewater using bimetal-chitosan, Sci. World J., 9 (2013) 476271, doi: 10.1155/2013/476271.
[3] L.X. Zhang, S.Y. Tang, F.X. He, Y. Liu, W. Mao, Y.T. Guan, Highly efficient and selective capture of heavy metals by poly(acrylic acid) grafted chitosan and biochar composite for wastewater treatment, Chem. Eng. J., 378 (2019) 122215, doi: 10.1016/j.cej.2019.122215.
[4] B.J. Pan, H. Qiu, B.C. Pan, G.Z. Nie, L.L. Xiao, L. Lv, W.M. Zhang, Q.X. Zhang, S.R. Zheng, Highly efficient removal of heavy metals by polymer-supported nanosized hydrated Fe(III) oxides: behavior and XPS study, Water Res., 44 (2010) 815–824.
[5] A. Eltaweil, I.M. Mamdouh, E.E. Monaem, G.E. Subruiti, Highly efficient removal for methylene blue and Cu^{2+} onto UiO-66 metal–organic framework/carboxylated graphene

oxideincorporated sodium alginate beads, ACS Omega, 6 (2021) 23528–23541.
[6] G. Asgari, B.R.S. Sahebi, Removal of a cationic dye from wastewater during purification by *Phoenix dactylifera*, Desal. Water Treat., 52 (2014) 7354–7365
[7] R. Foroutan, S.J. Peighambardoust, R. Mohammadi, S.H. Peighambardoust, B. Ramavandi, Development of new magnetic adsorbent of walnut shell ash/starch/Fe_3O_4 for effective copper ions removal: treatment of groundwater samples, Chemosphere, 96 (2022) 133978, doi: 10.1016/j.chemosphere.2022.133978.
[8] S. Dandil, D.A. Sahbaz, C. Acikgoz, Adsorption of Cu(II) ions onto crosslinked chitosan/waste active sludge char (WASC) beads: kinetic, equilibrium, and thermodynamic study, Int. J. Biol. Macromol., 136 (2019) 668–675.
[9] X.W. Song, Y.W. Cao, X.H. Bu, X.P. Luo, Porous vaterite and cubic calcite aggregated calcium carbonate obtained from steamed ammonia liquid waste for Cu^{2+} heavy metal ions removal by adsorption process, Appl. Surf. Sci., 536 (2021) 147958, doi: 10.1016/j.apsusc.2020.147958.
[10] Q.M. Kong, X.J. Wang, T. Lou, Preparation of millimeter-sized chitosan/carboxymethyl cellulose hollow capsule and its dye adsorption properties, Carbohydr. Polym., 244 (2020) 116481, doi: 10.1016/j.carbpol.2020.116481.
[11] W.J. Ren, J.K. Gao, C. Lei, Y.B. Xie, Y.R. Cai, Q.Q. Ni, J.M. Yao, Recyclable metal-organic framework/cellulose aerogels for activating peroxymonosulfate to degrade organic pollutants, Chem. Eng. J., 349 (2018) 766–774.
[12] L.Z. Qiao, S.S. Li, Y.L. Li, Y. Liu, K.F. Du, Fabrication of superporous cellulose beads via enhanced inner cross-linked linkages for high efficient adsorption of heavy metal ions, J. Cleaner Prod., 253 (2020) 120017, doi: 10.1016/j.jclepro.2020.120017.
[13] S. Gao, T.T. Luo, Q. Zhou, W.J. Luo, H.F. Li, L.R. Jing, Surface sodium lignosulphonate-immobilized sawdust particle as an efficient adsorbent for capturing Hg^{2+} from aqueous solution, J. Colloid Interface Sci., 517 (2018) 9–17.
[14] A.S. Eltaweil, G.S. Elgarhy, G.M. El-Subruiti, A.M. Omer, Carboxymethyl cellulose/carboxylated graphene oxide composite microbeads for efficient adsorption of cationic methylene blue dye, Int. J. Biol. Macromol., 154 (2020) 307–318.
[15] J.J. Wang, J. Wei, Facile synthesis of Zr(IV)-crosslinked carboxymethyl cellulose/carboxymethyl chitosan hydrogel using PEG as pore-forming agent for enhanced phosphate removal, Int. J. Biol. Macromol., 176 (2021) 558–566.
[16] H.Y. Yu, H.J. Hong, S.M. Kim, H.C. Ko, H.S. Jeong, Mechanically enhanced graphene oxide/carboxymethyl cellulose nanofibril composite fiber as a scalable adsorbent for heavy metal removal, Carbohydr. Polym., 240 (2020) 116348, doi: 10.1016/j.carbpol.2020.116348.
[17] M. Hosny, M. Fawzy, A.M. Abdelfatah, E.E. Fawzy, A.S. Eltaweil, Comparative study on the potentialities of two halophytic species in the green synthesis of gold nanoparticles and their anticancer, antioxidant and catalytic efficiencies, Adv. Powder Technol., 32 (2021) 3220–3233.
[18] M. Hosny, M. Fawzy, E.M. El-Fakharany, A.M. Omer, E.M. Abd El-Monaem, R.E. Khalifa, A.S. Eltaweil, Biogenic synthesis, characterization, antimicrobial, antioxidant, antidiabetic, and catalytic applications of platinum nanoparticles synthesized from *Polygonum salicifolium* leaves, J. Environ. Chem. Eng., 10 (2022) 106806, doi: 10.1016/j.jece.2021.106806.
[19] A.S. Eltaweil, H.A. Mohamed, E.M. Abd El-Monaem, G.M. El-Subruiti, Mesoporous magnetic biochar composite for enhanced adsorption of malachite green dye: characterization, adsorption kinetics, thermodynamics and isotherms, Adv. Powder Technol., 31 (2020) 1253–1263.
[20] K. Iamsaard, C.H. Weng, J.H. Tzeng, J. Anotai, A.R. Jacobson, Y.T. Lin, Systematic optimization of biochars derived from corn wastes, pineapple leaf, and sugarcane bagasse for Cu(II) adsorption through response surface methodology, Bioresour. Technol., 382 (2023) 129131, doi: 10.1016/j.biortech.2023.129131.
[21] F. Duan, Y. Zhu, Y. Liu, A. Wang, Fabrication of porous adsorbents from eco-friendly aqueous foam for high-efficient removal of cationic dyes and sustainable utilization assessment, J. Environ. Sci., 137 (2024) 395–406.
[22] C.L. Vieira, F.O.S. Neto, V.H. Carvalho-Silva, R. Signini, Design of a polar chitosan-type adsorbent for removal of Cu(II) and Pb(II): an experimental and DFT viewpoint of the complexation process, J. Environ. Chem. Eng., 7 (2019) 103070, doi: 10.1016/j.jece.2019.103070.
[23] M.E. Avval, P.N. Moghadam, M.M. Baradarani, Synthesis of a new nanocomposite based-on graphene-oxide for selective removal of Pb^{2+} ions from aqueous solutions, Polym. Compos., 40 (2019) 730–737.
[24] Y.Y. Ge, Z.L. Li, Application of lignin and its derivatives in adsorption of heavy metal ions in water: a review, ACS Sustainable Chem. Eng., 6 (2018) 7181–7192.
[25] H. Valdes, R.F. Tardon, C.A. Zaror, Methylene blue removal from contaminated waters using heterogeneous catalytic ozonation promoted by natural zeolite: mechanism and kinetic approach, Environ. Technol., 33 (2012) 1895–1903.
[26] F. Yu, Y. Li, S. Han, J. Ma, Adsorptive removal of antibiotics from aqueous solution using carbon materials, Chemosphere, 153 (2016) 365–385.
[27] X. Liu, G.R. Chen, D.J. Lee, T. Kawamoto, H. Tanaka, M.L. Chen, Y.K. Luo, Adsorption removal of cesium from drinking waters: a mini review on use of biosorbents and other adsorbents, Bioresour. Technol., 160 (2014) 142–149.
[28] Y. Li, F. Wang, Y.W. Miao, Y.L. Mai, H.L. Li, X.T. Chen, J.Z. Chen, A lignin-biochar, with high oxygen-containing groups for adsorbing lead ion prepared by simultaneous oxidization and carbonization, Bioresour. Technol., 307 (2020) 123165, doi: 10.1016/j.biortech.2020.123165.
[29] S.M. Shaheen, N.K. Niazi, N.E.E. Hassan, I. Bibi, H.L. Wang, D.C.W. Tsang, Y.S. Ok, N. Bolan, J. Rinklebe, Wood-based biochar for the removal of potentially toxic elements in water and wastewater: a critical review, Int. Mater. Rev., 64 (2019) 216–247.
[30] P. Li, S. Kim, J. Jin, D.H. Chun, J.H. Park, Efficient photo-degradation of volatile organic compounds by iron-based metal-organic frameworks with high adsorption capacity, Appl. Catal., B, 263 (2020) 118284, doi: 10.1016/j.apcatb.2019.118284.
[31] Q.W. Zhou, B.H. Liao, L.N. Lin, W.W. Qiu, Z.G. Song, Adsorption of Cu(II) and Cd(II) from aqueous solutions by ferromanganese binary oxide-biochar composites, Sci. Total Environ., 615 (2018) 115–122.
[32] C. Puri, G. Sumana, Highly effective adsorption of crystal violet dye from contaminated water using graphene oxide intercalated montmorillonite nanocomposite, Appl. Clay Sci., 166 (2018) 102–112.
[33] R K. Sharma, R. Kumar, A.P. Singh, Metal ions and organic dyes sorption applications of cellulose grafted with binary vinyl monomers, Sep. Purif. Technol., 209 (2019) 684–697.
[34] W. Fu, Z.Q. Huang, Magnetic dithiocarbamate functionalized reduced graphene oxide for the removal of Cu(II), Cd(II), Pb(II), and Hg(II) ions from aqueous solution: synthesis, adsorption, and regeneration, Chemosphere, 209 (2018) 449–456.
[35] M.R. Awual, Novel ligand functionalized composite material for efficient copper(II) capturing from wastewater sample, Composites, Part B, 172 (2019) 387–396.
[36] Y. Zhang, G.H. Huang, C.J. An, X.Y. Xin, X. Liu, M.Y. Raman, Y. Yao, X. Wang, M. Doble, Transport of anionic azo dyes from aqueous solution to gemini surfactant-modified wheat bran: synchrotron infrared, molecular interaction and adsorption studies, Sci. Total Environ., 595 (2017) 723–732.
[37] N.W. Cao, X.Y. Zhao, M.M. Gao, Z.Y. Li, X.J. Ding, C. Li, K.N. Liu, X.D. Du, W.X. Li, J. Feng, Y.M. Ren, T. Wei, Superior selective adsorption of MgO with abundant oxygen vacancies to removal and recycle reactive dyes, Sep. Purif. Technol., 275 (2021) 119236, doi: 10.1016/j.seppur.2021.119236.
[38] J.T. Tang, Y Song, F.P. Zhao, S. Spinney, J.D.S. Bernardes, K.C. Tam, Compressible cellulose nanofibril (CNF) based aerogels produced via a bio-inspired strategy for heavy metal ion and dye removal, Carbohydr. Polym., 208 (2019) 404–412.
[39] X. Li, X.H. Wang, T.T. Han, C. Hao, S.Q. Han, X.B. Fan, Synthesis of sodium lignosulfonate-guar gum composite hydrogel

for the removal of Cu^{2+} and Co^{2+}, Int. J. Biol. Macromol., 175 (2021) 459–472.
[40] Y J. Ding, J.D. Wu, J.Q. Wang, J.P. Wang, J.R. Ye, F. Liu, Superhydrophilic carbonaceous-silver nanofibrous membrane for complex oil/water separation and removal of heavy metal ions, organic dyes and bacteria, J. Membr. Sci., 614 (2020) 118491, doi: 10.1016/j.memsci.2020.118491.
[41] Y. Liu, M.S. Niu, X.L. Yi, G. Li, H. Zhou, W. Gao, Boron vacancies of mesoporous MnO_2 with strong acid sites, free Mn^{3+} species and macropore decoration for efficiently decontaminating organic and heavy metal pollutants in black-odorous waterbodies, Appl. Surf. Sci., 561 (2021) 150081, doi: 10.1016/j.apsusc.2021.150081.
[42] T. Hou, L. Yan, J. Li, Y. Yang, L. Shan, X. Meng, X. Li, Y. Zhao, Adsorption performance and mechanistic study of heavy metals by facile synthesized magnetic layered double oxide/carbon composite from spent adsorbent, Chem. Eng. J., 384 (2020) 123331, doi: 10.1016/j.cej.2019.123331.
[43] W.L. Zuo, Y.D. Yu, H. Huang, Making waves: microbe-photocatalyst hybrids may provide new opportunities for treating heavy metal polluted wastewater, Water Res., 195 (2021) 116984, doi: 10.1016/j.watres.2021.116984.
[44] M. Choudhary, R. Kumar, S. Neogi, Activated biochar derived from *Opuntia ficus-indica* for the efficient adsorption of malachite green dye, Cu^{2+} and Ni^{2+} from water, J. Hazard. Mater., 392 (2020) 122441, doi: 10.1016/j.jhazmat.2020.122441.